Updated Hybrid Lattice-Boltzmann Model for Low-Mach Reactive Flows

Muhammad Tayyab, Yongliang Feng, Pierre Boivin

UPDATED HYBRID LATTICE-BOLTZMANN MODEL FOR LOW-MACH REACTIVE FLOWS

M. Tayyab*, Y. Feng* and P. Boivin*
pierre.boivin@univ-amu.fr
*Aix Marseille Univ, CNRS, Centrale Marseille, M2P2, Marseille, France

Abstract
A Lattice-Boltzmann model for low-Mach reactive flows is presented, built upon our recently published model (Comb & Flame, 196, 2018). The approach is hybrid and couples a Lattice-Boltzmann solver for the resolution of mass and momentum conservation and a finite difference solver for the energy conservation. Having lifted the constant thermodynamic and transport properties assumptions, the model presented now fully accounts for the classical reactive flow thermodynamic closure: each component is assigned NASA coefficients for calculating its thermodynamic properties. A temperature-dependent viscosity is considered, from which are deduced thermo-diffusive properties via specification of Prandtl and component-specific Schmidt numbers. Other major improvements from our previous contribution include the consideration of the pressure work in the energy equation, as well as detailed kinetics. Validation is carried out through simulation of the planar freely propagating flame and the growth of the associated Darrieus-Landau instability.

Introduction

Motivated by the rapid development of Lattice-Boltzmann (LB) methods in the field of low-Mach external aerodynamics and aeroacoustics [1], and particularly its potential as an engineering tool [2–6] we recently proposed a hybrid LB framework able to tackle combustion in low-Mach flows [7] in line with the quest of extending the LB capabilities to reactive flows [8–14].

Based on nearest neighbor lattices, our model's implementation is straight-forward, but assumes a constant heat capacity for the mixture, a stark limitation when temperatures above 1000K are encountered. Neglecting the pressure work term in the energy conservation equation, written in temperature form, is a second strong assumption of our previous contribution [7]. This contribution aims at lifting these two limitations as to make the model fully functional for the simulation of reactive flows, including detailed chemistry description.

This is achieved through consideration of the classical thermodynamic closure based on NASA polynomial coefficients [15], as used in CHEMKIN [16], or CANTERA [17]. Chemistry is accounted for, through a 12-step mechanism for H_2-air combustion [18] derived from the San Diego mechanism [19]. Each of the nine species is assigned a Schmidt number relating its diffusion property with a temperature-dependent viscosity coefficient. Thermal diffusion is accounted for via a Prandtl number as in [20].

Validation is carried out by comparisons with Cantera computations [17] in premixed configurations. To further demonstrate the capability of the model, the Darrieus-Landau instability is simulated, and the associated growth-rate is compared with asymptotic descriptions [21–23], showing excellent agreement for the linear onset of the instability.

The paper is organized as follows. First, the LB combustion model is presented, with extensive implementation details. The model is then systematically validated, with results compared to Cantera computations [17]. Conclusions and future perspectives are then discussed.

A hybrid Lattice Boltzmann combustion model

In line with our initial combustion model proposal [7], this new contribution consists of a Lattice Boltzmann (LB) solver coupled with a Finite Difference (FD) solver. This Section presents successively the LB solver, responsible for the resolution of mass and momentum conservation, the FD solver, responsible for the resolution of energy and species conservation, and details on their two-way coupling.

Mass and momentum conservation: Lattice Boltzmann approach

The LB solver part is identical to that of our previous contribution [7], with the exception of data exchanges. The equations and resolution procedure are nonetheless reminded hereafter.

The mass and momentum conservation equations read

$$\begin{cases} \dfrac{\partial \rho}{\partial t} + \dfrac{\partial}{\partial x_\alpha}(\rho u_\alpha) & = 0, \\ \dfrac{\partial \rho u_\alpha}{\partial t} + \dfrac{\partial}{\partial x_\beta}(\rho u_\alpha u_\beta) & = -\dfrac{\partial p}{\partial x_\alpha} + \dfrac{\partial}{\partial x_\beta}\Big[\mu(\dfrac{\partial u_\alpha}{\partial x_\beta} + \dfrac{\partial u_\beta}{\partial x_\alpha} - \dfrac{2}{3}\dfrac{\partial u_\gamma}{\partial x_\gamma}\delta_{\alpha\beta})\Big], \end{cases} \tag{1}$$

where ρ is the local density, u_α the velocity vector, p the pressure, μ is the dynamic viscosity and $\delta_{\alpha\beta}$ is the Kronecker symbol. Computation of the pressure p in (1) requires the choice of a thermodynamic closure. This work considers a multicomponent ideal gas, and the pressure reads

$$p = \rho \overline{r} T, \tag{2}$$

where $\overline{r} = R/\overline{W}$; R being the gas constant and $\overline{W}$ the mean molecular weight, obtained as

$$1/\overline{W} = \sum_k Y_k / W_k, \tag{3}$$

with Y_k the k-th component mass fraction, and W_k its molecular weight.

Instead of these classical variables, Lattice-Boltzmann methods consider the probability density function $f(\boldsymbol{x}, \boldsymbol{c}, t)$ for a particle to be at position $\boldsymbol{x}$, velocity $\boldsymbol{c}$ and instant t. The n-dimensional velocity space is then discretized into m discrete velocities $c_{i\alpha}$, forming the standard $\mathrm{D_nQ_m}$ lattice tensor with characteristic velocity c_s [24, 25]. The macroscopic quantities in lattice units relate with the m probability density functions $f_i(x_\alpha, t)$ as

$$\rho = \sum_{i=1}^{m} f_i, \quad \rho u_\alpha = \sum_{i=1}^{m} c_{i\alpha} f_i. \tag{4}$$

Following the Chapman-Enskog technique [26], one can show the asymptotic equivalence between solving the continuous formulation (1) and solving the Bhatnagar-Gross-Krook (BGK) model [27]

$$f_i(x_\alpha + c_{i\alpha}\delta t, t + \delta t) - f_i(x_\alpha, t) = -\frac{1}{\tau}[f_i(x_\alpha, t) - f_i^{eq}(x_\alpha, t)] \tag{5}$$

where τ is a non-dimensional relaxation time, δt is the time-step and f_i^{eq} is the i-th equilibrium distribution function corresponding to the Maxwell-Boltzmann distribution [28], here

expanded up to the third-order:

$$
\begin{aligned}
&f_i^{eq} = \rho w_i \big[1 + \frac{c_{i\alpha}u_\alpha}{c_s^2} + \frac{A^{(2)}_{\alpha\beta}Q^{(2)}_{i\alpha\beta}}{2c_s^4} + \frac{A^{(3)}_{\alpha\beta\gamma}Q^{(3)}_{i\alpha\beta\gamma}}{6c_s^6}\big],\\
&A^{(2)}_{\alpha\beta} = u_\alpha u_\beta + (\theta-1)c_s^2\delta_{\alpha\beta}, \quad Q^{(2)}_{i\alpha\beta} = c_{i\alpha}c_{i\beta} - c_s^2\delta_{\alpha\beta},\\
&A^{(3)}_{\alpha\beta\gamma} = u_\alpha u_\beta u_\gamma + (\theta-1)c_s^2[u\delta]_{\alpha\beta\gamma}, \quad Q^{(3)}_{i\alpha\beta\gamma} = c_{i\alpha}c_{i\beta}c_{i\gamma} - c_s^2[c\delta]_{\alpha\beta\gamma}.
\end{aligned}
\tag{6}
$$

In the above, $[c\delta]_{\alpha\beta\gamma} = c_\alpha\delta_{\beta\gamma} + c_\beta\delta_{\alpha\gamma} + c_\gamma\delta_{\alpha\beta}$ and θ is the non-dimensional temperature

$$\theta = \frac{\overline{r}T}{c_s^2} = \frac{RT}{c_s^2}\sum_k \frac{Y_k}{W_k}. \tag{7}$$

The single relaxation time, required in the resolution of the discrete Boltzmann equation (5), can now be defined as

$$\tau = \frac{\mu}{\rho\theta c_s^2\delta t} + \frac{1}{2}, \tag{8}$$

with the viscosity μ being assigned a temperature-dependent value following a power-law

$$\mu = \mu_0\left(\frac{T}{T_0}\right)^\beta. \tag{9}$$

Lattice Boltzmann variables can be converted to physical units for length, time, mass and temperature following the same relations as in our previous work [7]. For instance, $\delta t = \delta x.\frac{c_s}{c_{sp}}$, where c_{sp} is the reference physical sound speed.

Energy and species conservation: finite difference approach
The energy and species conservation are solved through a classical finite difference approach. As in [7], the N species conservation equations read

$$\frac{\partial Y_k}{\partial t} + u_\alpha\frac{\partial}{\partial x_\alpha}Y_k = \frac{1}{\rho}\frac{\partial}{\partial x_\alpha}(-\rho V_{k,\alpha}) + \frac{\dot{\omega}_k}{\rho}, \tag{10}$$

with $\dot{\omega}_k$ the chemical source term for species k. In our work, we use one of the simplest models for the species diffusion velocity

$$V_{k,\alpha} = -D_k\frac{\partial X_k}{\partial x_\alpha}\frac{W_k}{\bar{W}} + V^c_\alpha Y_k, \tag{11}$$

X_k being k-th species mole fraction. Note that a more detailed transport model, e.g. [29, 30], may be considered instead, should the application require it. The diffusion coefficient D_k is defined via a component specific Schmidt number Sc_k as a function of the viscosity

$$D_k = \frac{\mu}{\rho Sc_k}. \tag{12}$$

and V_α^c is the correction velocity [31]

$$V_\alpha^c = \sum_{k=1}^{N} D_k \frac{\partial X_k}{\partial x_\alpha} \frac{W_k}{\overline{W}} \tag{13}$$

ensuring the global mass conservation.

As to lift the constant heat capacity C_p limitation of [7], it was found easier to now consider an energy conservation equation (in place of the temperature equation) due to its simpler and arguably more classical form [31]. Among the many energy equations forms [31], we went for the internal energy form (sensible + chemical):

$$e = \sum_{k=1}^{N} Y_k e_k(T), \quad e_k = \int_{T_0}^{T} C_{v,k}(T) dT - \frac{RT_0}{W_k} + \Delta h_{f,k}^o, \tag{14}$$

associated to the following corresponding energy equation

$$\frac{\partial e}{\partial t} + u_\alpha \frac{\partial e}{\partial x_\alpha} = -\frac{1}{\rho} \frac{\partial q_\alpha}{\partial x_\alpha} + \frac{\sigma_{\alpha\beta}}{\rho} \frac{\partial u_\alpha}{\partial x_\beta}. \tag{15}$$

where the viscous and pressure tensors are combined into $\sigma_{\alpha\beta}$ as in [31]

$$\sigma_{\alpha\beta} = \tau_{\alpha\beta} - p\delta_{\alpha\beta} = -p\delta_{\alpha\beta} - \frac{2}{3}\mu \frac{\partial u_\gamma}{\partial x_\gamma} \delta_{\alpha\beta} + \mu\left(\frac{\partial u_\alpha}{\partial x_\beta} + \frac{\partial u_\beta}{\partial x_\alpha}\right). \tag{16}$$

Lastly the heat flux q_α reads

$$q_\alpha = -\lambda \frac{\partial T}{\partial x_\alpha} + \rho \sum_{k=1}^{N} h_k Y_k V_{k,\alpha}, \tag{17}$$

where

$$h_k = \int_{T_0}^{T} C_{p,k}(T) dT + \Delta h_{f,k}^o, \tag{18}$$

and the thermal conductivity λ is defined as a function of the viscosity and the Prandtl number

$$\lambda = \frac{\mu}{Pr} \sum_{k=1}^{N} Y_k C_{p,k}. \tag{19}$$

The thermodynamic properties required for the thermodynamic closure are specified in the form of the classical NASA polynomials [15] for each species k.

Note that alternative energy conservation equations are indeed equivalent to (15) under continuous form [31], but not necessarily in filtered form. As part of this model's development, it is worth mentioning that we have implemented and tested the conservation equation for sensible energy, i.e. Eq. (14) without formation enthalpy $\Delta h_{f,k}^o$, without noticeable change regarding the model's validity or numerical stability.

Implementation: two-way coupling between the LB and FD solvers

The implementation of the presented model is rather straight-forward and follows the same logic as in our initial version [7]. The algorithm flowchart is reminded in Fig. 1, updated

to this new version. The idea is that, at every time-step, the FD solver communicates the updated non-dimensional temperature θ to the LB solver, for use in the equilibrium function computation (6). Simultaneously, the LB solver communicates to the FD solver updated values for the density ρ and velocity vector u_α.

LB solver specifics
Within a time-step, solving the LB approach can be done directly through (5). Although not required for the test cases presented in the following section, we recommend the use of a source term to correct for the defect of symmetry of the third-order moment on standard lattices, modifying (5) into

$$\begin{aligned} f_i(x_\alpha + c_{i\alpha}\delta t, t+\delta t) &= f_i(x_\alpha, t) - \tfrac{1}{\tau}[f_i(x_\alpha, t) - f_i^{eq}(x_\alpha, t)] \\ &\quad +(1-\tfrac{1}{2\tau})s_i \end{aligned} \tag{20}$$

where the external force term s_i reads [32, 33]

$$s_i = \frac{w_i}{2c_s^4}\Big\{Q_{ixx}\frac{\partial}{\partial x}[\rho u_x(1-\theta-u_x^2)] + Q_{iyy}\frac{\partial}{\partial y}[\rho u_y(1-\theta-u_y^2)]\Big\}. \tag{21}$$

Similarly, inclusion of a regularization step is also recommended [34, 35].

FD solver specifics
The choice of discrete operator for solving the discrete form of Eqs (10) and (15) is fundamental in the overall model stability. The isotropic finite difference operators [36] are used in the following Section. Regarding temporal integration, forward euler, RK2 and RK4 have been implemented, with no effect on the validation carried out in the next Section. RK2 has our preference in order to keep consistency with the LB solver, which is second-order in time [25].

Boundary conditions
The LB inlet boundary is based on the standard bounce back scheme [37]. Alternatively, the LB inlet boundary may be implemented following the regularized non-equilibrium bounce back scheme presented in [38]. For the validations carried out in the following Section, the inlet boundary conditions on the FD solver are hard-coded (fixed) for species and energy. Outlet boundary conditions are treated as zero gradient. Periodic or symmetric boundary conditions are used for the walls.

Validation test cases
The hybrid Lattice-Boltzmann combustion model was implemented in the D_2Q_9 framework, and validation simulations were carried out, in premixed configurations. The reference solutions provided for comparison were obtained with the Cantera software [17], with use of the same transport and thermodynamic properties.

H_2*-air combustion model*
Throughout this Section, we consider the 12-step skeletal mechanism for H_2-air combustion [18] derived from the detailed San Diego mechanism [19]. The mechanism, summarized in Table 1, involves eight reacting species, as well as inert N_2 for combustion with air. The associated thermodynamic data was obtained from the San Diego mechanism website [19]. The various parameters required for the computation of the viscosity through (9) as well as

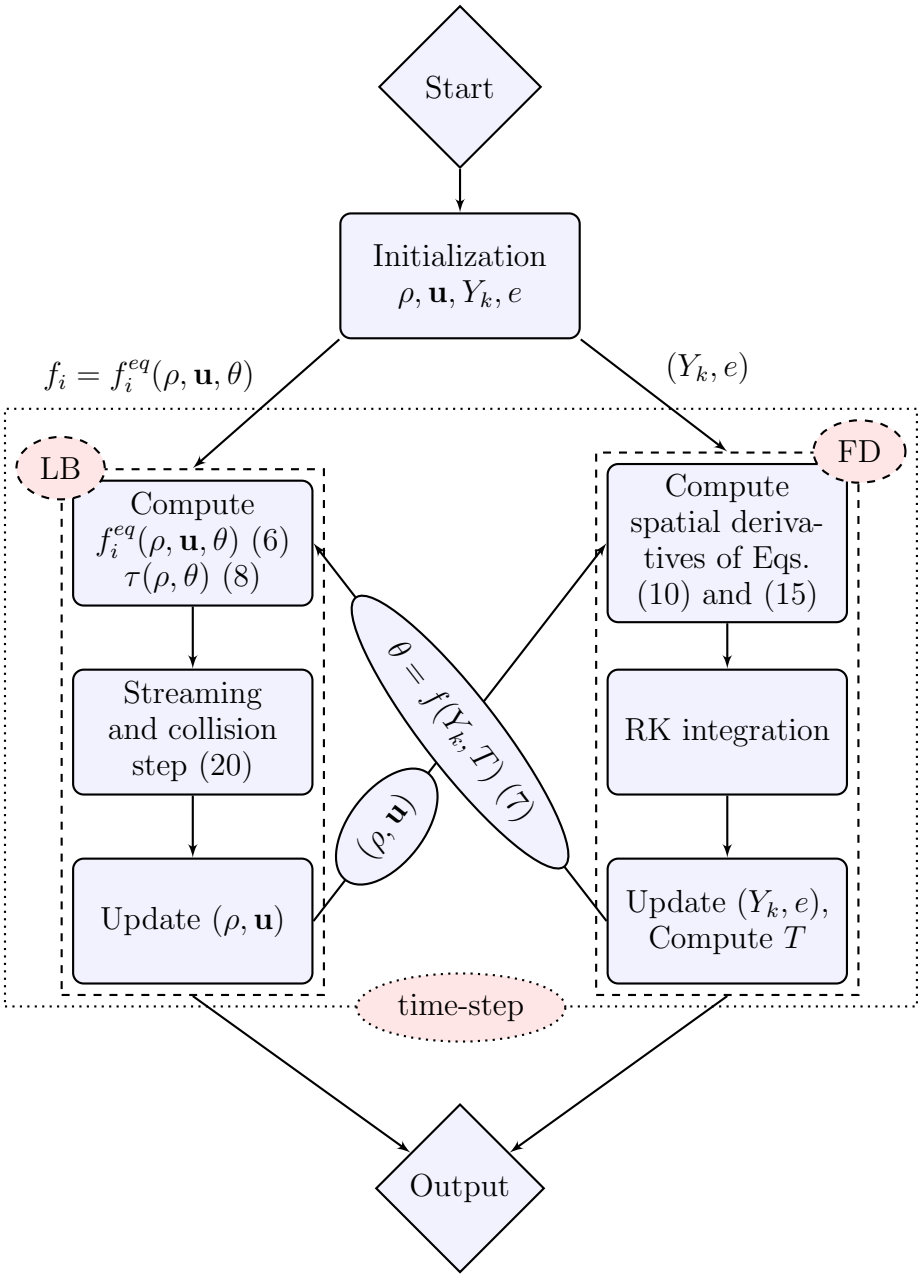

Figure 1: The algorithm proposed consists of a Lattice-Boltzmann (LB) solver coupled with a classical Finite Differences (FD) solver. Data exchanges between the two solvers are clearly identified.

Table 1: The 12-step skeletal mechanism for the combustion of H_2-air [18]. Up-to-date rates are available [19].

1	$H + O_2 \rightleftharpoons OH + O$	7	$HO_2 + OH \rightarrow H_2O + O_2$
2	$H_2 + O \rightleftharpoons OH + H$	8	$H + OH + M \rightleftharpoons H_2O + M$
3	$H_2 + OH \rightleftharpoons H_2O + H$	9	$2\ H + M \rightleftharpoons H_2 + M$
4	$H + O_2 + M \rightarrow HO_2 + M$	10	$2\ HO_2 \rightarrow H_2O_2 + O_2$
5	$HO_2 + H \rightarrow 2\ OH$	11	$HO_2 + H_2 \rightarrow H_2O_2 + H$
6	$HO_2 + H \rightleftharpoons H_2 + O_2$	12	$H_2O_2 + M \rightarrow 2\ OH + M$

species (12) and heat (19) diffusion properties are those recommended in Cerfacs' database [39] and validated for this mechanism. They are reported in Table 2.

Table 2: Power-law's viscosity coefficients (SI units), Prandtl number and Schmidt numbers for each species of the 12-step mechanism.

μ_0	1.8405×10^{-5}	β	0.6759
Pr	0.7500	Sc_{H_2}	0.2100
Sc_H	0.1400	Sc_{O_2}	0.8000
Sc_{OH}	0.5300	Sc_O	0.5300
Sc_{H_2O}	0.6000	Sc_{HO_2}	0.8000
$Sc_{H_2O_2}$	0.8200	Sc_{N_2}	1.0000

1D freely propagating flame

Let us now consider the standard freely propagating flame configuration, following the same setup as in [7]. The computational domain is pseudo one-dimensional of length L, with a height corresponding to three cells and grid size of 1.0×10^{-5} m. At the left of the domain, the velocity is set to an arbitrary value U_f, and the right boundary is left open (zero gradient). Periodic boundary conditions are applied to the top and bottom limits.

The inital conditions, reported in Table 3, consists of two half-domains with a sharp transition at $L/2$. The left hand-side of the domain corresponds to the fresh gases, whereas the right hand-side corresponds to the burnt gases initialized at the corresponding thermo-chemical equilibrium, computed with Cantera [17]. As in our previous contribution [7], we measure the flame speed as

$$S_L = U_f - \frac{\rho_f U_f - \rho_b U_b}{\rho_f - \rho_b}, \tag{22}$$

where the subscript f represents fresh and b burnt state of the gases, respectively the first and last cell of the computational domain. History of this expression (22) is monitored until convergence to the flame velocity [7].

The results obtained are compared with Cantera reference computations in Fig. 2.a. The temperature and mass fractions profiles show an excellent agreement, including for the minor species H and HO_2, whose profiles in the flame appear indistinguishable from the reference. The equivalence ratio of the fresh gases was then modified as to obtain Fig. 2.b, again showing an excellent agreement for the flame velocity as a function of the equivalence ratio.

Table 3: Initial conditions: 1-D domain is initialized with fresh gases corresponding to $(0 : L/2)$ and burnt gases $(L/2 : L)$

Variables	$0 : L/2$	$L/2 : L$
T	300.000 K	2385.000 K
p	1.000 atm	1.000 atm
u	0.000	0.000
Y_{H_2}	2.852×10^{-2}	1.145×10^{-3}
Y_{H}	0.000	6.983×10^{-5}
Y_{O_2}	2.264×10^{-1}	7.474×10^{-3}
Y_{OH}	0.000	5.458×10^{-3}
Y_{O}	0.000	3.838×10^{-4}
Y_{H_2O}	0.000	2.403×10^{-1}
Y_{HO_2}	0.000	1.074×10^{-6}
$Y_{H_2O_2}$	0.000	1.444×10^{-10}
Y_{N_2}	7.451×10^{-1}	7.451×10^{-1}

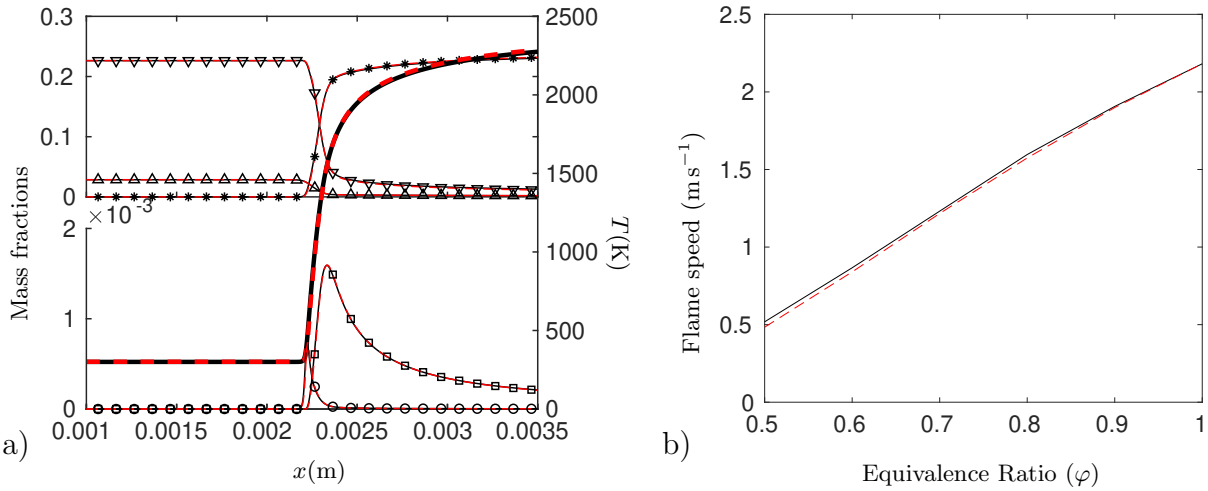

Figure 2: Freely propagating flame: a) Temperature profile (thick line), H_2 ($\triangle$), O_2 ($\triangledown$), H_2O ($*$), H ($\square$), HO_2 ($\circ$) mass fractions. Fresh gases are in stoichiometric proportion, at 300K and atmospheric pressure. b) Variation with equivalence ratio of the corresponding flame speed. Cantera reference (plain line), and present model (red dashed line).

2D Darrieus-Landau instability

To conclude the validation of our model, let us study the intrinsic instability of the premixed flame presented in previous sub-section. The pseudo one-dimensional computational domain is now extended to a fully two-dimensional domain with grid size of 1.11×10^{-5} m. At $t = 0$, the 2D domain is initialized with the profiles obtained from the 1D computation reported in Fig. 2.a. The front position, defined as the maximum temperature gradient position is then perturbed with a wavenumber (k) of 600m^{-1}. The evolution of the front position is reported in Fig. 3.a. It is interesting to note that the evolution produces the expected behavior,

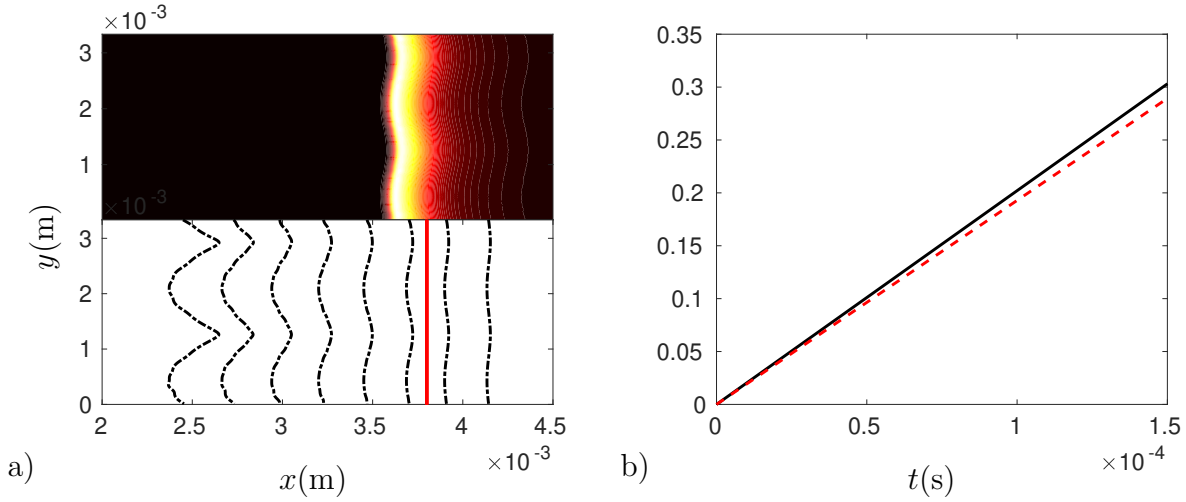

Figure 3: 2-D Darrieus Landau instability. a) Representation of the expansion with interval $\delta t = 1.111\ 10^{-4}$s and $k = 600\text{m}^{-1}$. The front is initially at $x \approx 4.5$mm. The vertical line marks the end of the linear regime depicted in plot b. b) Comparison of analytical (plain line) and simulated growth rate (dashed line) in the linear region delimited ending at the vertical line in plot a.

and that the coupling between the LB and FD solvers is robust to more complex flame front shapes. Note that increased stability has been obtained through regularization of the collision operator [38].

Figure 3.b concludes the validation of the model by comparing the growth rate in the linear regime with the analytical solution [21–23]. As expected, the amplitude of the perturbation A grows exponentially from its initial value A_0 according to

$$A = A_0 e^{\omega t}, \tag{23}$$

with ω the perturbation growth rate. Theory indicates that, in the linear regime [21–23],

$$\omega = S_L k \frac{-\sigma + \sqrt{\sigma^3 + \sigma^2 - \sigma}}{\sigma + 1}, \tag{24}$$

with k the wave number and $\sigma = \rho_f / \rho_b = 6.822$ the ratio between the fresh and burnt gases density.

Concluding remarks

A new hybrid Lattice-Boltzmann model for the simulation of reactive flows has been presented. Mass and momentum conservation are addressed within a Lattice-Boltzmann solver, whereas the energy conservation is addressed via a classical finite difference solver.

Major improvements from our initial proposal [7] include the consideration of detailed kinetics and a more complete thermodynamic closure, where the species thermodynamic properties are set individually via the classical NASA polynomials.

Heat and molecular diffusion are also accounted for via introduction of Prandtl and Schimdt numbers, related to a user-specified temperature-dependent viscosity coefficient. Validation of the model was carried out based on a 1D planar freely propagating flame test case and a 2D simulation of the Darrieus-Landau thermo-diffusive intrinsic instability.

Future work will include application of the model to more complex, three-dimensional configurations.

Acknowledgements

P. Haldenwang is gratefully acknowledged for fruitful discussions on thermo-diffusive instabilities.

This work was granted access to the HPC resources of Aix-Marseille Université funded by the project Equip@Meso (ANR-10-EQPX-29-01), and from GENCI-TGCC/CINES (Grant 2018-A0032A07679). We also acknowledge support from Labex MEC (ANR-10-LABX-0092) and the A*MIDEX project (ANR-11-IDEX-0001-02), funded by the "Investissements d'Avenir".

References

[1] Chen, S.Y., Doolen, G.D., "Lattice boltzmann method for fluid flows", *Annual Review of Fluid Mechanics* 30:329–364 (1998).

[2] D'Hooge, A., Rebbeck, L., Palin, R., Murphy, Q., Gargoloff, J., Duncan, B., "Application of real-world wind conditions for assessing aerodynamic drag for on-road range prediction", Tech. rep., SAE Technical Paper (2015).

[3] Gleason, M.E., Duncan, B., Walter, J., Guzman, A., Cho, Y.C., "Comparison of computational simulation of automotive spinning wheel flow field with full width moving belt wind tunnel results", *SAE International Journal of Passenger Cars-Mechanical Systems* 8:275–293 (2015).

[4] Khorrami, M.R., Fares, E., Duda, B., Hazir, A., "Computational evaluation of airframe noise reduction concepts at full scale", *22nd AIAA/CEAS Aeroacoustics Conference*, p. 2711 (2016).

[5] Khorrami, M.R., Fares, E., "Simulation-based airframe noise prediction of a full-scale, full aircraft", *22nd AIAA/CEAS aeroacoustics conference*, p. 2706 (2016).

[6] Casalino, D., Hazir, A., Mann, A., "Turbofan broadband noise prediction using the lattice boltzmann method", *AIAA Journal* pp. 1–20 (2017).

[7] Feng, Y., Tayyab, M., Boivin, P., "A lattice-boltzmann model for low-mach reactive flows", *Combustion and Flame* 196:249 – 254 (2018).

[8] Filippova, O., Hänel, D., "A Novel Lattice BGK Approach for Low Mach Number Combustion", *Journal of Computational Physics* 158:139–160 (2000).

[9] Yamamoto, K., Takada, N., "LB simulation on soot combustion in porous media", *Physica A: Statistical Mechanics and its Applications* 362:111–117 (2006).

[10] Chiavazzo, E., Karlin, I.V., Gorban, A.N., Boulouchos, K., "Coupling of the model reduction technique with the lattice boltzmann method for combustion simulations", *Combustion and Flame* 157:1833–1849 (2010).

[11] Xu, A., Lin, C., Zhang, G., Li, Y., "Multiple-relaxation-time lattice boltzmann kinetic model for combustion", *Physical Review E* 91:043306 (2015).

[12] Sun, K., Yang, S., Law, C.K., "A diffuse interface method for simulating the dynamics of premixed flames", *Combustion and Flame* 163:508–516 (2016).

[13] Ashna, M., Rahimian, M.H., Fakhari, A., "Extended lattice boltzmann scheme for droplet combustion", *Physical Review E* 95:053301 (2017).

[14] Hosseini, S.A., Darabiha, N., Thévenin, D., "Mass-conserving advection–diffusion lattice boltzmann model for multi-species reacting flows", *Physica A: Statistical Mechanics and its Applications* 499:40–57 (2018).

[15] Esch, D., Siripong, A., Pike, R., "Thermodynamic properties in polynomial form for carbon, hydrogen, nitrogen, and oxygen systems from 300 to 15000 k", *NASA technical report* (1970).

[16] Kee, R., Rupley, F., Miller, J., "The chemkin thermodynamic data base", Tech. rep., Sandia National Labs., Livermore, CA (USA) (1990).

[17] Goodwin, D.G., Moffat, H.K., Speth, R.L., "Cantera: An object-oriented software toolkit for chemical kinetics, thermodynamics, and transport processes", `http://www.cantera.org` (2017), version 2.3.0.

[18] Boivin, P., Jiménez, C., Sánchez, A.L., Williams, F.A., "An explicit reduced mechanism for H_2–air combustion", *Proceedings of the Combustion Institute* 33:517–523 (2011).

[19] Williams, F., et al., "Chemical-kinetic mechanisms for combustion applications, University of California, San Diego", *http://web.eng.ucsd.edu/mae/groups/combustion/mechanism.html* (2018).

[20] Schönfeld, T., Rudgyard, M., "Steady and unsteady flows simulations using the hybrid flow solver avbp", *AIAA Journal* 37:1378–1385 (1999).

[21] Denet, B., Haldenwang, P., "Numerical study of thermal-diffusive instability of premixed flames", *Combustion science and technology* 86:199–221 (1992).

[22] Denet, B., Haldenwang, P., "A numerical study of premixed flames darrieus-landau instability", *Combustion science and technology* 104:143–167 (1995).

[23] Matalon, M., "Intrinsic flame instabilities in premixed and nonpremixed combustion", *Annu. Rev. Fluid Mech.* 39:163–191 (2007).

[24] Mohamad, A.A., *Lattice Boltzmann method: fundamentals and engineering applications with computer codes*, Springer Science & Business Media, 2011.

[25] Krüger, T., Kusumaatmaja, H., Kuzmin, A., Shardt, O., Silva, G., Viggen, E.M., *The Lattice Boltzmann Method: Principles and Practice*, Springer, 2016.

[26] Chapman, S., Cowling, T.G., *The Mathematical Theory of Non-Uniform Gases*, Cambridge University Press, 1970.

[27] Bhatnagar, P.L., Gross, E.P., Krook, M., "A model for collision processes in gases. i. small amplitude processes in charged and neutral one-component systems", *Phys. Rev.* 94:511–525 (1954).

[28] Shan, X.W., Yuan, X.F., Chen, H.D., "Kinetic theory representation of hydrodynamics: a way beyond the navier-stokes equation", *Journal of Fluid Mechanics* 550:413–441 (2006).

[29] Ern, A., Giovangigli, V., *Multicomponent transport algorithms*, vol. 24, Springer Science & Business Media, 1994.

[30] Ern, A., Giovangigli, V., "Eglib: A general-purpose fortran library for multicomponent transport property evaluation", *Manual of EGlib version* 3:12 (2004).

[31] Poinsot, T., Veynante, D., *Theoretical and numerical combustion*, RT Edwards, Inc., 2005.

[32] Feng, Y., Sagaut, P., Tao, W., "A three dimensional lattice model for thermal compressible flow on standard lattices", *Journal of Computational Physics* 303:514–529 (2015).

[33] Feng, Y., Sagaut, P., Tao, W.Q., "A compressible lattice Boltzmann finite volume model for high subsonic and transonic flows on regular lattices", *Computers and Fluids* 131:45–55 (2016).

[34] Feng, Y.L., Guo, S.L., Tao, W.Q., Sagaut, P., "Regularized thermal lattice Boltzmann method for natural convection with large temperature differences", *International Journal of Heat and Mass Transfer* 125:1379–1391 (2018).

[35] Jacob, J., Malaspinas, O., Sagaut, P., "A new hybrid recursive regularised bhatnagar–gross–krook collision model for lattice boltzmann method-based large eddy simulation", *Journal of Turbulence* pp. 1–26 (2018).

[36] Kumar, A., "Isotropic finite-differences", *Journal of Computational Physics* 201:109 – 118 (2004).

[37] Yu, D., Mei, R., Shyy, W., "Improved treatment of the open boundary in the method of lattice boltzmann equation: general description of the method", *Progress in Computational Fluid Dynamics, an International Journal* 5:3–12 (2004).

[38] Malaspinas, O., Chopard, B., Latt, J., "General regularized boundary condition for multi-speed lattice Boltzmann models", *Computers & Fluids* 49:29–35 (2011).

[39] "Cerfacs online database for cantera", `http://www.cerfacs.fr/cantera/` (2018).